Design of plate and screw anchors in dense sand

Cerfontaine, Benjamin; Knappett, Jonathan; Brown, Michael; Bradsaw, Aaron S.

Published in:
7th International Symposium on Deformation Characteristics of Geomaterials (IS-Glasgow 2019)

DOI:
10.1051/e3sconf/20199216010

Publication date:
2019

Design of plate and screw anchors in dense sand: failure mechanism, capacity and deformation

Benjamin Cerfontaine[1,*], *Jonathan* Knappett[1], *Michael* Brown[1], and *Aaron* Bradshaw[2]

[1]University of Dundee, School of Science and Engineering, DD1 4HN, Dundee, United Kingdom
[2]University of Rhode Island, Civil and Environmental Engineering, Kingston, RI 02881, United States

Abstract. Plate and screw anchors provide a significant uplift capacity and have multiple applications in both onshore and offshore geotechnical engineering. Uplift design methods are mostly based on semi-empirical approaches assuming a failure mechanism, a normal and a shear stress distribution at failure and empirical factors back-calculated against experimental data. However, these design methods are shown to under- or overpredict most of the existing larger scale experimental tests. Numerical FE simulations are undertaken to provide new insight into the failure mechanism and stress distribution which should be considered in anchor design in dense sand. Results show that a conical shallow wedge whose inclination to the vertical direction is equal to the dilation angle is a good approximation of the failure mechanism in sand. This shallow mechanism has been observed in each case for relative embedment ratios (depth/diameter) ranging from 1 to 9. However, the stress distribution varies non-linearly with depth, due to the soil deformability and progressive failure. A sharp peak of normal and shear stress can be identified close to the anchor edge, before a gradual decrease with increasing distance along the shear plane. The peak stress magnitude increases almost linearly with embedment depth at larger relative embedment ratios. Although further research is necessary, these results lay the basis for the development of a new generation of design criteria for determining anchor capacity at the ultimate limiting state.

1 Introduction

Plate and screw anchors are mainly used in geotechnical engineering to secure man-made structures against significant uplift loads. They are mainly used onshore to stabilise light structures such as transmission towers [1] or residential buildings [2]. Plate anchors are already used to secure mooring lines to the seabed for floating offshore structures [3] while screw anchors have been recently proposed as an efficient foundation system for offshore renewable energy systems [4].

Plate anchors are composed of a single plate that is installed into the ground through drag embedment (VLA), suction embedment (SEPLA) or a driven pile [3]. Plate anchors can provide a combined lateral and vertical capacity for loads which are inclined, as the plate rotates ('keys') to be perpendicular to the direction of load application. Screw anchors are composed of one or several helices attached to a shaft. They are literally screwed into the soil through the application of a torque combined with a vertical 'crowd' force in order to ensure a constant rotation to advancement rate [5]. The uplift capacity is mainly provided by the helix, whose reaction with the soil generates a wedge-type shallow failure mechanism, similar to a plate anchor.

The uplift capacity design of these anchors mainly relies on semi-analytical approaches [6-9] based on 1g field or small-scale tests. Their formulation, usually based on limit analysis, requires the definition of an assumed failure mechanism, a stress distribution along it and one or several empirical factors.

The objective of this work is to provide insight into the uplift failure mechanism and stress distribution along it, by comparison of numerical simulations and the various semi-analytical approaches available. The final goal is to provide sufficient information to develop the next-generation of design criteria, based on a more physically-based stress-distribution rather than global empirical factors.

2 (Semi-) Analytical approaches

The semi-analytical design approaches are mostly based on limit analysis, whose formulations are reviewed and summarised in [10]. These approaches usually depend on two main hypotheses: the definition of a failure mechanism and the stress distribution along it at the ultimate limit state (plastic collapse mechanism). The criteria proposed by Ghaly [11], Mitsch and Clemence [7], Meyerhof [6] and Murray and Geddes [12] all introduce an empirical factor calibrated against experimental tests, while the approach of Giampa does not [9].

* Corresponding author: b.cerfontaine@dundee.ac.uk

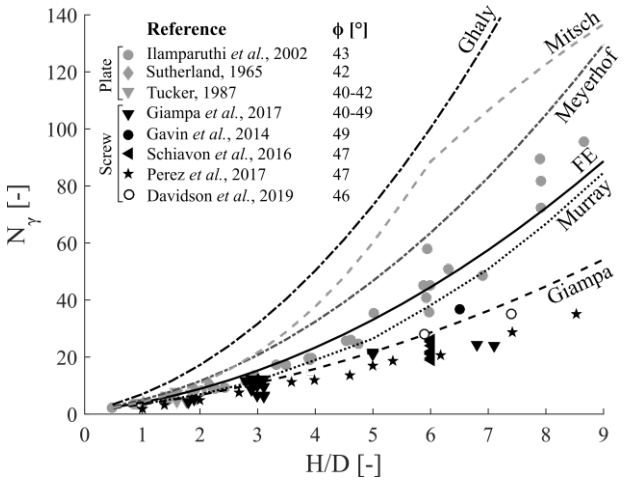

Fig. 2. Evolution of the non-dimensional bearing factors $N\gamma$ as a function of the relative embedment ratio *H/D*. Experimental results (small-scale 1g or centrifuge, field tests, [6], [8], [14–19]) are denoted by a marker, numerical (FE) results by a solid line and analytical criteria assuming (ϕ_p=47°, ψ_p=18°) by a discontinuous line.

A non-dimensional bearing factor N_γ is usually defined to compare uplift capacities F_y related to different geometries and soil densities

$$N_\gamma = \frac{F_y}{\gamma' AH} \quad (1)$$

where γ' is the buoyant unit weight, A is the plate area (=$\pi D^2/4$), D is the plate diameter and H is the embedment depth.

Results of semi-analytical approaches for a plate anchor embedded in dense sand are compared in Fig. 2 to experimental data from the literature (small-scale 1g and centrifuge, field tests). The comparison of these values shows that there is significant variability amongst the semi-analytical criteria and three of them clearly overpredict the uplift capacity. This is most probably due to the calibration of empirical variables based on small-scale 1g models within which soil dilatancy is more pronounced due to lower effective confining stress, leading to larger predicted values [13]. It should be noted that overprediction or underprediction of the experimental results is also a function of the friction angle, some criteria providing better estimate at larger or lower values.

Therefore, finite element simulations have been carried out to investigate the difference between the approaches and understand which hypotheses (failure mechanism, stress distribution) are valid for dense sands.

3 Definition of the FE model

The idealisation of the problem is shown in **Fig 1**, where a plate anchor of diameter D (=1.7m) is assumed to be wished-in-place at an embedment depth equal to H and has a rigid body imposed vertical displacement (u_y). The case study considered here corresponds to upscaling of an anchor for offshore applications [4]. The problem is discretised into finite elements in PLAXIS 2D [14] and simulations are conducted axisymmetrically. The soil domain is discretised into 15-node triangular elements while 5-node plate elements are used to model the steel structure. 5-node interface elements are added between plate and soil elements to allow gap opening (no tension condition) and sliding. Boundary conditions are set far enough from the anchor to avoid boundary effects (7*D* below the anchor, 17*D* laterally [10]). The soil was assumed fully saturated, but the loading was deemed slow enough to ensure fully drained conditions. The mesh was chosen to be a good compromise between results accuracy and CPU time [10].

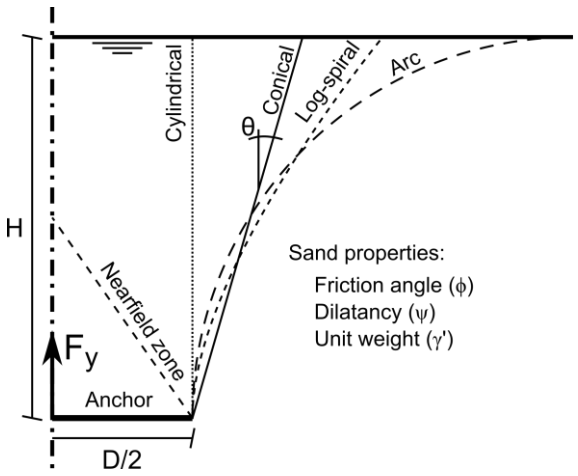

Fig 1. Idealisation of the anchor uplift and different assumed failure mechanisms

The 'hardening soil with small strain stiffness' (HSsmall) [15] model was chosen as a constitutive law for the soil. Simulations using this model have already been successfully validated against field experiments [16-17] and its parameters have been extensively calibrated against laboratory tests for HST95 sand, across a large range of relative densities [18]. The sand relative density considered here is equal to 90%.

The HSsmall model is based on the hardening of a Mohr-Coulomb surface (based on shear strain) and a cap surface (based on volumetric strain). The stiffness is confinement dependent and decreases as strain increases. The volumetric behaviour is non-associated and depends on the dilation angle. A tension cut-off avoids any traction of the material while the dilatancy cut-off ensures the material void ratio remains lower than e_{max}.

A detailed description of the parameters is given in [10] while a summary of the most important features is given in Table 1.

4 Results

4.1 Load-displacement relationship

Uplift simulations of plate anchors embedded in dense sand and relative embedment ratios ranging from 1 to 9 were carried out. The load-displacement relationships corresponding to uplift simulations of plates in a dense sand are depicted in Fig. 4. Failure for each simulation can be assumed when a plateau is reached in the load-displacement relationship (Fig. 4) and a failure mechanism is fully formed (discussed later). Results show

that the bearing capacity (at failure) is always increasing with relative embedment ratio *H/D*, as depicted in Fig. 4. These numerical results are consistent with experimental results, as shown in Fig. 2 (black solid line).

Table 1. HSsmall parameters for the HST95 Congleton sand, after [18], ϕ_p is the peak friction angle, ψ_p is the peak dilation angle, e_0 is the initial void ratio and γ_{tot} the saturated unit weight

e_0 **[-]**	0.497
ψ_p **[°]**	18.5
ϕ_p **[°]**	47
γ_{tot} **[kN/m³]**	20.42

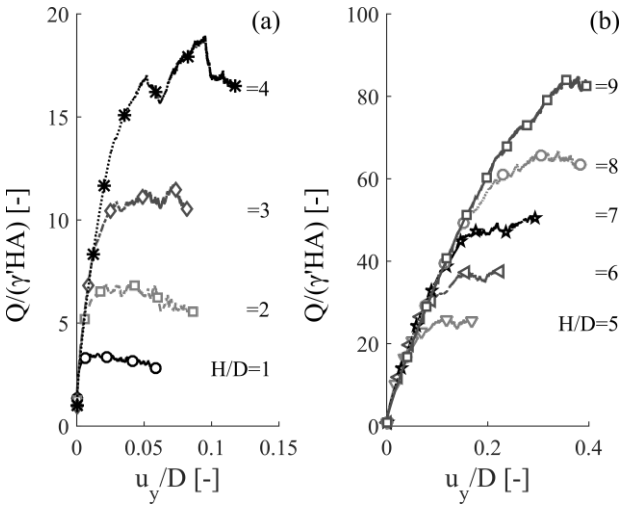

Fig. 4. Normalised load Q - displacement u_y relationships for simulations in dense sand (D_r 90%) for relative embedment ratios *H/D* ranging from (a) 1 to 4 and (b) 5 to 9. Vertical scales are different.

The continuous increase of the bearing capacity contradicts the transition commonly proposed between shallow and deep failure mechanisms, leading to a limitation of bearing capacity. According to the common definition, it exists a critical depth after which the failure is a flow around mechanism, which limits the evolution of the bearing factor as the relative embedment increases. Meyerhof & Adams [6] provided a peak friction angle dependent relationship to define this transition H/D, which should be between 8 and 9 for the considered friction angle. However, according to Mitsch & Clemence [7], this transition relative depth H/D should be 5.

However, the displacement required to fully form the failure mechanism and reach a plateau might be up to 0.4*D*. It is common practice in geotechnical engineering to define failure as the maximum load mobilised at a given displacement (e.g. 0.1*D*).

4.2 Failure mechanism

There is no general agreement on the actual shape of the uplift shallow failure mechanism, as many parameters can influence it, such as the embedment depth [19] or the installation method [20]. Several mathematical shapes (cylindrical, conical, logarithmic spiral) have been proposed, as shown Fig 1, but the conical surface, defined by a straight line, is the most frequently used. However, there is no consensus on the inclination this failure mechanism should have with respect to the vertical. For instance, Meyerhof and Adams use $\phi_p/3$ [6], Mitsch and Clemence $\phi_p/2$ [7] while Giampa et al. assumed the inclination was equal to the peak dilation angle ψ_p [9] and undertook some FE simulations and limit equilibrium analyses to verify the assumption.

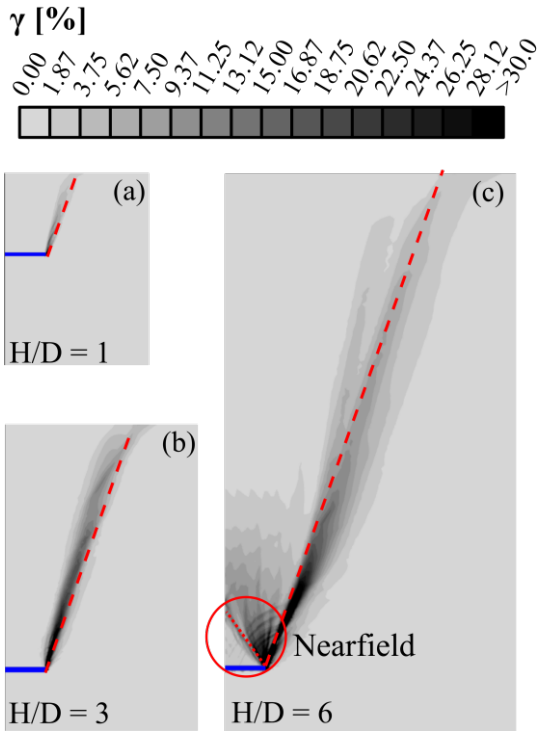

Fig. 3. Comparison of shear strain (γ) contours obtained numerically at peak load for three relative embedment ratios.

The zone of intense shear strain was traced and analysed for all numerical results to identify the failure mechanism, with examples depicted in Fig. 3. In this figure, results are traced for a selected time step. This time step corresponds to the peak load attained in Fig. 4. In addition, the maximum shear strain plotted was limited to 30% for readability of the figure, though it could be larger locally.

Firstly, it should be noted that a shallow failure mechanism (extending up to the surface) was always observed, whatever the relative embedment depth. This echoes the comments made in the previous section where the bearing capacity is always increasing without showing a clear shallow to deep transition.

Secondly, at the lowest relative embedment ratios, the observed failure mechanism is very close to a straight line inclined at the dilation angle to the vertical direction, as assumed by Giampa [9] (e.g. Fig. 3(a-c)). This assumption is drawn in Fig. 3 as a dashed line, emerging from the plate edge.

As the relative embedment ratio increases, the failure mechanism diverges from a straight line, although it remains close. This divergence occurs at *H/D* = 5.5. The new shape of the failure mechanism tends to extend more laterally, as shown in Fig. 3(c). In addition, a diffuse shear strain zone (referred as nearfield) develops just above the plate anchor (Fig. 3(c)) and increases in size and

magnitude with *H/D*. It describes an approximately conical soil block (dotted line in Fig. 3(c)), similar to the one forming beneath shallow foundations.

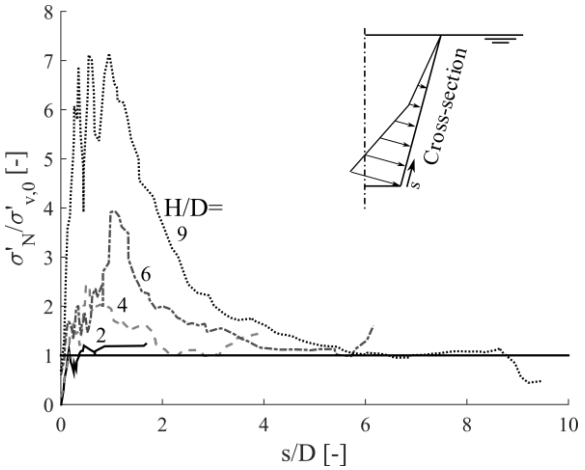

Fig. 5. Normalised normal stress distribution along a cross-section emanating from the plate edge and inclined at the dilation angle ψ_p to the vertical, at different relative embedment ratios H/D

4.3 Stress distribution

Most of the semi-analytical approaches previously presented assume that the stress distribution along the failure surface is defined such that

$$\sigma'_N = K\gamma' z \qquad (2)$$

where K is a coefficient that has been defined as either equal to the passive earth coefficient K_p [6], or as a modified coefficient $K'_p(\delta)$ based on an average mobilised friction angle δ [11], or as a function of the friction and dilation angles $K(\phi_p,\psi_p) = \cos(\phi_p - \psi_p)$ [9].

An estimation of the stress distribution at failure can be obtained for the numerical results. A cross-section is obtained by the software through interpolation of the stress field within the soil elements. The cross-section was assumed to be along a straight line starting from the plate edge and inclined at ψ_p to the vertical direction (Giampa hypothesis). Both normal and shear stresses can be obtained.

As an example, the normal stress is provided for the at four relative embedment ratios *H/D* (respectively 2, 4, 6 and 9) in Fig. 5. The variable *s* represents the distance from the edge of the plate in the cross-section direction and is normalised with respect to the helix diameter. The normal stress is normalised with respect to the initial vertical effective stress $\sigma'_{v0}=\gamma' z$.

While the stress distribution is typically assumed to be linearly increasing in existing model, Fig. 5 shows that the normal stress distribution is non-linear. As the embedment increases, a peak appears in the normal stress distribution, close to the anchor edge.

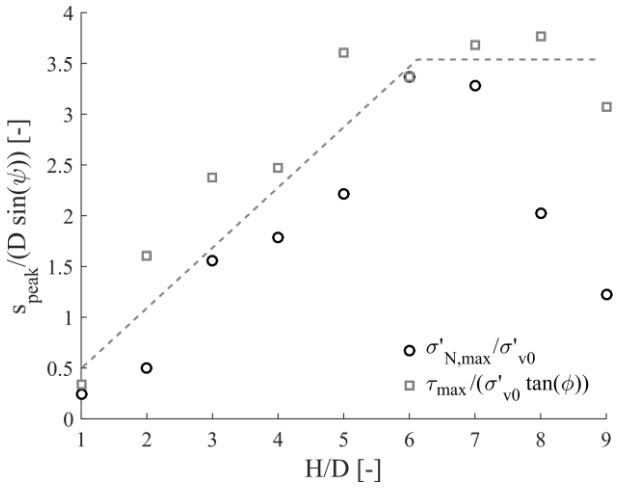

Fig. 6. Normalised distance from the plate edge at which the maximum normal or shear stress occurs as a function of relative embedment ratio *H/D*

4.4 Generalisation

The stress distribution non-linearity is the consequence of the soil compressibility and the relatively large displacement required to fully form the failure mechanism, particularly at large *H/D*. The behaviour of a rigid soil wedge, as considered in conventional limit equilibrium analysis, can be idealised as shown in Fig. 6(a). The shear strain is identical all along the failure surface, as the vertical u_y displacement is identical for all points belonging to the soil wedge. Consequently, friction is mobilised first close to the surface and the maximum uplift load is reached as soon as the maximum shear stress is attained at the edge of the anchor.

For a deformable soil, a gradient of vertical displacement u_y exists, as illustrated in Fig. 6(b). It is larger close to the plate and decreases close to the soil surface. The lateral strain that should result from the vertical strain is restrained, which increases the lateral stress distribution, as shown in Fig. 7 for $H/D = 4$. As a consequence, the normal stress along the failure mechanism increases as well as the maximum shear stress. This stress enhancement is limited to a zone close to the anchor.

Subsequently, a larger displacement must be imposed to a deformable soil to fully form the failure mechanism. In addition, friction is mobilised first close to the plate edge, while it is mobilised first close to the surface in case of a rigid body.

Such an influence of the soil compressibility was originally recognised by Vesic [21] who introduced a compressibility factor I_r into his bearing factor definition. However, Vesic solution is based on a simple linear elasto-plastic model that does not take dilatancy into account.

Results depicted in Fig. 5 can be traced for all relative embedment ratios. The normal stress distribution can be characterised as depicted in Fig. 6(c). It increases rapidly to reach a peak normal stress ($\sigma'_{N,peak}$) at a distance (s_{peak}) from the plate edge. It decreases more slowly with

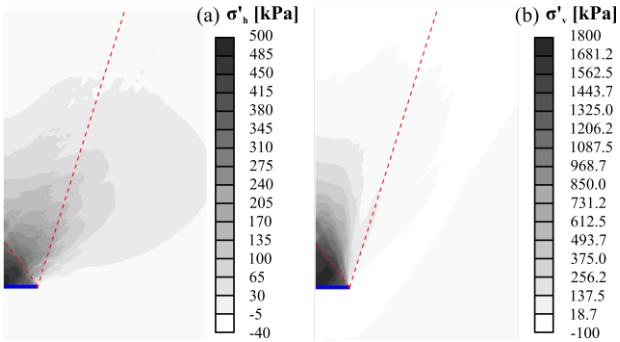

Fig. 7. Contour of (a) horizontal σ'_h and (b) vertical σ'_v cartesian effective stresses (positive compression) at failure, $H/D = 4$.

distance thereafter until it reaches a quasi-linear distribution. A similar trend can be observed for the shear stress distribution.

The peak normal and shear stresses for each simulation has been identified and is depicted in Fig. 8 as a function of the relative embedment ratio. The normal stress is normalised with respect to the maximum initial vertical stress ($\sigma'_{v0}=\gamma' H$) along the failure surface while the shear stress is normalised by a maximum friction ($\sigma'_{v0} \tan \phi$).

At relatively low embedment ratios (H/D = 1 or 2), there is no clear peak stress, as can be confirmed by the analysis of the normal stress cross-sections (similar to Fig. 5). As the relative embedment increases, the normalised peak stress increases almost linearly with the relative embedment ratio. This transition can be linked to the observed failure mechanism and the development of nearfield diffuse shear strain (Fig. 3 (c)).

The trend for the shear stress is almost identical to the normal stress, although the slopes of the linear trends are slightly different. The normalised ratios for peak and normal stress are also different. It is unclear whether this is due to interpolation inaccuracies (in tracing the cross-section) or if this results from another physical phenomenon.

The distance from the plate edge at which the peak stress (normal or shear) develops also increases with

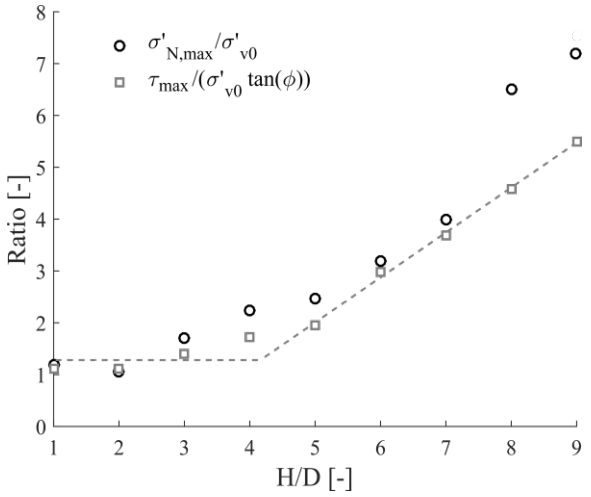

Fig. 8. Normalised peak normal stress $\sigma'_{N,max}$ and shear stress τ_{max} along the failure mechanism as a function of relative embedment ratio H/D

relative embedment ratio, as depicted in Fig. 6. There is a clear linearly increasing trend at low H/D, but there is greater scatter in the peak location at larger embedment depths ($H/D \geq 6$). Results in Fig. 6 could indicate that a plateau is reached at larger embedment depths.

5 Conclusion

In this work, FE simulations of circular flat plates embedded in dense sand at different embedment ratios have been undertaken. The analysis of the failure mechanism described by the induced shear strains in the soil has shown that the failure mechanism can be described as a shallow wedge, even at large embedment depth, whose inclination to the vertical direction can be assumed equal to the dilation angle. Nonetheless this assumed mechanism diverges from a straight line as relative embedment ratio increases.

The stress distribution along the failure mechanism was shown to be different from all existing semi-analytical approaches. The progressive failure and soil deformability induce a non-linear stress distribution (normal and shear) along the failure mechanism that must be taken into account to define a reliable analytical failure criterion. The shape of the stress distribution can be characterised by its peak (magnitude and distance from the plate edge) and its change with distance from the plate edge. The difference to existing solutions becomes more pronounced at increasing depths, which is consistent with greater soil compression associated with increased plate bearing stress acting on a longer column of soil. Although some approximate trends have been highlighted as a function of the relative embedment ratio, further research is necessary to better understand and describe it, for instance as a function of the compressibility parameters of the soil and soil density.

The definition of an accurate stress distribution along the slip plane for limit analysis approaches is more robust than the definition of a global empirical factor and opens new possibilities for the development of improved design methods. For instance, shear strain distribution along the failure mechanism could be obtained similarly along the same cross-section. Direct shear test results could then be used to determine if shear strain at different points along the slip surface is sufficient to trigger shear localisation and softening in certain regions, which could then be incorporated into analytical calculations.

This project has received funding from the European Union's Horizon 2020 research and innovation programme under the Marie Skłodowska-Curie grant agreement No 753156.

References

[1] C. H. C. Tsuha, J. M. S. Filho, and T. da Costa Santos, **15**, July, pp. 1–50, 2015.
[2] M. Sakr, *Can. Geotech. J.*, **46**, 9, pp. 1046–1061, 2009.
[3] C. Gaudin, M. J. Cassidy, C. D. O'Loughlin, Y. Tian, D. Wang, and S. Chow, *Int. J. Offshore Polar Eng.*, **27**, 1, pp. 44–53, 2017.
[4] C. Davidson *et al.*, submitted for publication in

Géotechnique, 2018.
[5] H. A. Perko, "Helical Piles: A Practical Guide to Design and Installation," 1 Edition. John Wiley & Sons, 2009.
[6] G. G. Meyerhof and J. I. Adams, *Can. Geotech. J.*, **5**, 4, 1968.
[7] M. P. Mitsch and S. . Clemence, "The uplift capacity of helix anchors in sand," in *Uplift behavior of anchor foundations in soil*, 1985, pp. 26–47.
[8] E. F. Murray and J. D. Geddes, *ASCE J. Geotech. Eng.*, **113**, 3, pp. 202–215, 1987.
[9] J. Giampa, A. Bradshaw, and J. Schneider, *Int. J. Geomech.*, **17**, 2, p. 4016056, 2017.
[10] B. Cerfontaine, J. A. Knappett, M. J. Brown, and A. S. Bradshaw, *Comput. Geotech.*, 2019.
[11] A. Ghaly, A. Hanna, and M. Hanna, *J. Geotech. Eng.*, **117**, 5, pp. 773–793, 1991.
[12] E. J. Murray and J. D. Geddes, "Resistance of Passive Inclined Anchors," *Geotechnique*, **39**, 3. pp. 417–431, 1989.
[13] A. Bradshaw *et al.*, *Geotech. Test. J.*, **39**, 6, pp. 1006–1014, 2016.
[14] PLAXIS, "PLAXIS 2D Tutorial Manual." Delft, The Netherlands, 2017.
[15] T. Schanz, A. Vermeer, and P. Bonnier, *Beyond 2000 Comput. Geotech. 10 years PLAXIS Int. Proc. Int. Symp. beyond 2000 Comput. Geotech. Amsterdam Netherlands 1820 March 1999*, p. 281, 1999.
[16] A. Tolooiyan and K. Gavin, *Geotech. Eng. Proc. Inst. Civ. Eng.*, **166**, pp. 549–560, 2013.
[17] J. A. Knappett, K. Caucis, M. J. Brown, J. R. Jeffrey, and J. D. Ball, *Proc. Inst. Civ. Eng. - Geotech. Eng.*, **169**, 5, pp. 436–454, 2016.
[18] A. H. Al-Defae, K. Caucis, and J. A. Knappett, *Géotechnique*, **63**, 14, pp. 1230–1244, 2013.
[19] J. Y. Liu, M. L. Liu, and Z. D. Zhu, *J. Geotech. Geoenvironmental Eng.*, **138**, 6, pp. 728–737, 2012.
[20] Z. A. Perez, J. A. Schiavon, C. H. C. Tsuha, D. Dias, and L. Thorel, *Can. Geotech. J.*, pp. 1–45, 2017.
[21] N. Vesic, "Breakout resistance of objects embedded in ocean bottom," 1969.